# Multi-scale Material Parameter Identification Using LS-DYNA® and LS-OPT®

Nielen Stander[1], Anirban Basudhar[1], Ushnish Basu[1], Imtiaz Gandikota[1], Vesna Savic[2], Xin Sun[3], Kyoo Sil Choi[3], Xiaohua Hu[3], Farhang Pourboghrat[4], Taejoon Park[4], Aboozar Mapar[4], Sharvan Kumar[5], Hassan Ghassemi-Armaki[5], Fadi Abu-Farha[6]

[1]Livermore Software Technology Corporation, Livermore CA, USA
[2]General Motors Company, Detroit MI, USA
[3]Pacific Northwest National Laboratory, Richland WA, USA
[4]Michigan State University, East Lansing MI, USA
[5]Brown University, Providence RI, USA
[6]Clemson University, Clemson SC, USA

## 1 Introduction

Ever-tightening regulations on fuel economy, and the likely future regulation of carbon emissions, demand persistent innovation in vehicle design to reduce vehicle mass. Classical methods for computational mass reduction include sizing, shape and topology optimization. One of the few remaining options for weight reduction can be found in materials engineering and material design optimization. Apart from considering different types of materials, by adding material diversity and composite materials, an appealing option in automotive design is to engineer steel alloys for the purpose of reducing plate thickness while retaining sufficient strength and ductility required for durability and safety.

A project to develop computational material models for advanced high strength steel is currently being executed under the auspices of the United States Automotive Materials Partnership (USAMP) funded by the US Department of Energy. Under this program, new Third Generation Advanced High Strength Steel i.e. 3GAHSS are being designed, tested and integrated with the remaining design variables of a benchmark vehicle Finite Element model. The objectives of the project are to integrate atomistic, microstructural, forming and performance models to create an integrated computational materials engineering (ICME) toolkit for 3GAHSS.

The mechanical properties of Advanced High Strength Steels (AHSS) are controlled by many factors, including phase composition and distribution in the overall microstructure, volume fraction, size and morphology of phase constituents as well as stability of the metastable retained austenite phase. The complex phase transformation and deformation mechanisms in these steels make the well-established traditional techniques obsolete, and a multi-scale microstructure-based modeling approach following the ICME [1] strategy was therefore chosen in this project.

Multi-scale modeling as a major area of research and development is an outgrowth of the Comprehensive Test Ban Treaty of 1996 which banned surface testing of nuclear devices [2]. This had the effect that experimental work was reduced from large scale tests to multiscale experiments to provide material models with validation at different length scales. In the subsequent years industry realized that multi-scale modeling and simulation-based design were transferable to the design optimization of any structural system.

Horstemeyer [2] lists a number of advantages of the use of multiscale modeling. Among these are: the reduction of product development time by alleviating costly trial-and-error iterations as well as the reduction of product costs through innovations in material, product and process designs. Multi-scale modeling can reduce the number of costly large scale experiments and can increase product quality by providing more accurate predictions. Research tends to be focussed on each particular length scale, which enhances accuracy in the long term.

This paper serves as an introduction to the LS-OPT® and LS-DYNA® methodology for multi-scale modeling. It mainly focuses on an approach to integrate material identification using material models of different length scales. As an example, a multi-scale material identification strategy, consisting of a Crystal Plasticity (CP) material model and a homogenized State Variable (SV) model, is discussed and

the parameter identification of the individual material models of different length scales is demonstrated. The paper concludes with thoughts on integrating the multi-scale methodology into the overall vehicle design.

## 2 New user material models in LS-DYNA®

Two constitutive models were implemented as user materials. These two models represent the two length scales respectively.

### 2.1 The MSU Crystal Plasticity model (Michigan State University)

The Combined Constraints Crystal Plasticity model [3] which is based on the principle of maximum dissipation is used to model the large plastic deformation in single crystals.

This model uses an optimization method to define a crystal plasticity based yield function. Crystal orientation is taken into account through the definition of Euler angles: ψ, θ, φ. The following hardening equation is used to model the flow stress [4,5]:

$$\dot{\tau}^{\alpha} = \sum_{\beta=1}^{N} h^{\alpha\beta} \left| \dot{\gamma}^{\beta} \right| \tag{1}$$

This equation states that slip on any slip system β contributes to the shear stress on a slip system α. Here $\dot{\gamma}^{\beta}$ is the shear strain increment on a slip system β and $\dot{\tau}^{\alpha}$ is the increment of shear stress on a slip system α. $h^{\alpha\beta}$ is the hardening moduli matrix and has the following form [5]:

$$h^{\alpha\beta} = h^{\beta}\left[q + (1-q)\delta^{\alpha\beta}\right] \tag{2}$$

Here $\delta^{\alpha\beta}$ is the Kronecker delta, $1 \leq q \leq 1.4$, and $h^{\beta}$ is defined as [5]:

$$h^{\beta} = h_0 \left| 1 - \frac{\tau_0^{\beta}}{\tau_s^{\beta}} \right|^{a} sgn\left(1 - \frac{\tau_0^{\beta}}{\tau_s^{\beta}}\right) \tag{3}$$

in which $h_0$ is a constant that defines the hardening rate, $a$ is the hardening exponent and $\tau_0^{\beta}$ is the critical resolved shear stress on a slip system $\beta$. The value of $\tau_0^{\beta}$ evolves during the deformation until it reaches $\tau_s^{\beta}$ which is the saturation value of the resolved shear stress on the slip system $\beta$.

### 2.2 State Variable model (Pacific Northwest National Laboratory)

PNNL has developed a State Variable model using the phase properties obtained from the CP model. A simple model is used to homogenize the Young's modulus, Poisson ratio, plastic modulus and volume fraction of each phase respectively. Phase stress-strain curves can be provided from the lower length-scale modeling (in this case CP) results or from experimental methods such as in-situ High Energy X-ray Diffraction (HEXRD) test. As for the phase transformation, the Olsen-Cohen model [6] is used as a phenomenological phase transformation kinetics model with the evolution of the austenitic volume fraction defined by:

$$V_{tm} = V_{a0}[1 - \exp\{-b[1 - \exp(-a\bar{\varepsilon}_p)]^n\}] \tag{4}$$

where $a$, $b$, and $n$ can be determined by fitting with the experimentally obtained phase transformation kinetics under different loading conditions.

The original model developed by PNNL was implemented in LS-DYNA and enhanced in the following aspects:

1. The consistent tangent stiffness was implemented for implicit analysis. This is required in the larger design optimization problem which involves vehicle performance and requires modal frequency properties. The material identification process is also significantly accelerated by not having to use explicit dynamic analysis.
2. A Newton iteration scheme was implemented to compute the plastic consistency parameter.

3. The material was extended to shell elements by implementing a Newton iteration scheme for enforcing the plane stress condition. This iteration scheme is necessary in LS-DYNA because for the Hughes-Liu shells, a Jaumann stress update results in a non-zero normal stress being provided to the material routine. Because of this, the common alternate approach of analytically projecting the stress to the plane-stress space is inadequate.

## 3 Integration of the MSU-CP model with the PNNL-SV model in LS-OPT

Because of the interdependency of the material parameters, calibration of the PNNL-SV model relies on the calibrated MSU-CP model parameters as inputs. Thererefore, a multi-level process is required to integrate the models. Different stages [7] are required in order to sequence the two parameter identification tasks which are accompanied by multiple test cases to incorporate the four metal phases and five triaxial load cases. Different levels [7] are required because, to calibrate the two models, optimization stages are involved in the process flow and have to be controlled from an outer level.

The process is depicted in Figure 1 and is summarized as follows:

1. Parameter identification of the MSU-CP model using single grain micropillar tests::
    a. Choose a material model from the available lattice options: FCC, BCC-12, BCC-24, BCC-48. The code after the word BCC represents the number of the slip systems implemented in the model. These can be set in the MSU-CP model.
    b. Obtain experimental force-displacement curves for each of ferrite, austenite, martensite and newly transformed martensite phases. Micropillar tests are used for ferrite and martensite. A single grain with pre-determined orientation is used for generating the calibration test data in order to avoid the complexity associated with relative orientations of multiple grains.
    c. Construct finite element (FE) models for the micro-pillar experiments used to determine the force-displacement curves.
    d. Using 4 parameter identification runs, one for each phase, determine the strain-hardening parameters $\tau_{0i},\ \tau_{Si},\ h_{0i},\ a_i,\ i = 1,2,3$ for each phase. The remaining parameters are assumed to be constant.
2. Simulation of the 4 polygranular models using the afore-optimized MSU-CP model:
    a. Determine an average output stress-strain curve using a polycrystal FE model for each phase. A polycrystal model consists of a meshed representative volume, e.g. cube, with multiple grains. Each grain has a random orientation given by randomized Euler angles of the integration points. The Euler angles are randomized internally when the appropropriate option is selected.
3. Parameter identification of the State Variable Model:
    a. Obtain experimental retained austenitic volume fraction vs. equivalent plastic strain curves for 5 triaxial stress states: (bi-axial, compression, tension, plane strain and shear).
    b. Feed the 4 output stress-strain curves from the 4 previous polycrystal runs into the PNNL-SV model. If computational stress-strain curves are not available due to unavailability of single grain CP calibration data, experimental curves for polycrystal test samples can be used.
    c. Execute a parameter identification run to determine $a_i$,$b_i$,$n_i$ for each triaxial load case $i$. The Olsen-Cohen formula [Eq. (4)] is used for this purpose.
4. Data Processing and sheet metal forming:
    a. Use response-variables [7] to convert the 5 $a$, $b$, $n$ values to $\boldsymbol{a}$, $\boldsymbol{b}$ and $\boldsymbol{n}$ curves with respect to triaxiality values, each with 5 points. The curves for $a$, $b$ and $n$ with respect to triaxiality define the final SV model that can be used for an LS-DYNA metal forming or crash analysis. In case all 5 values are not available, a smaller number can also be used to define each curve.

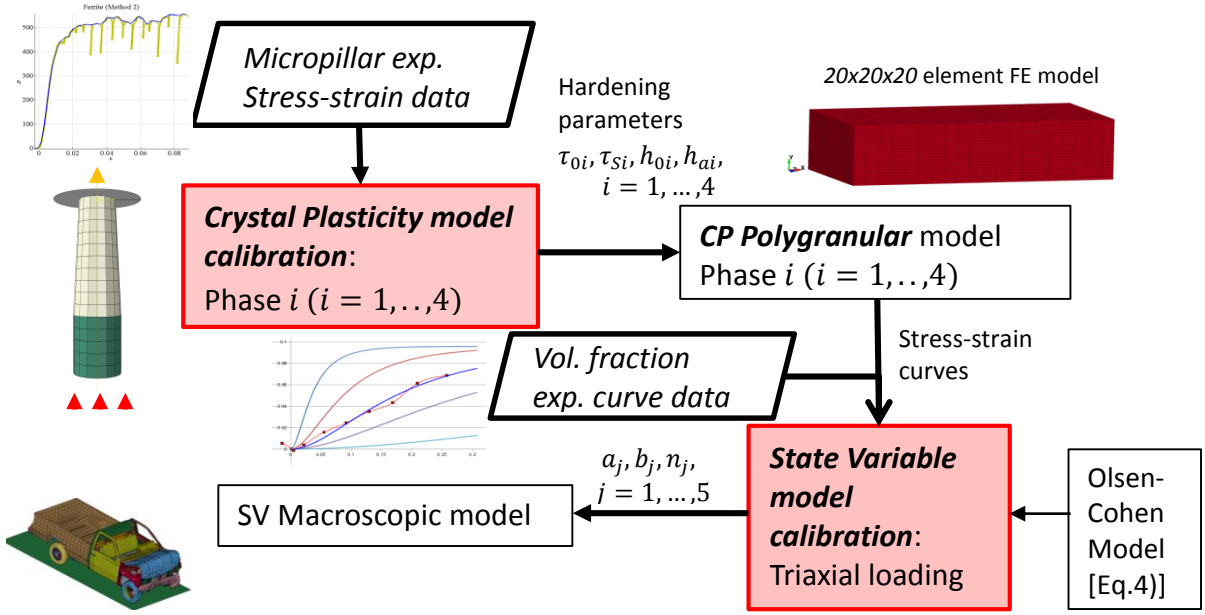


*Fig.1: Process flow of the integrated multi-scale calibration of Crystal Plasticity and State Variable models*

## 4 Calibration of the MSU Crystal Plasticity model using LS-DYNA and LS-OPT

To gain an understanding of the calibration of each phase and loading, each calibration was first studied as an isolated individual component.

The calibration of the Crystal Plasticity BCC-24 model was conducted with LS-OPT using the ferrite and martensite phases. The experiments are done on single grain micropillar structures of which tip displacement and force results are extracted. A micropillar constitutes a pure crystal structure representing a single phase and is in the form of a tapered cylinder with measurements in the 1 micron range. BAO QP980 steel was used in the experiments.

### 4.1 Preparation of the experimental data

Experimental stress-strain test results for the Ferritic and Martensitic phases were obtained from Brown University. The two respective sets of compression stress-strain results are shown in Figure 2(a). The results are based on the Force-Displacement results where stress $\sigma = \frac{4F}{\pi D^2}$ and strain $\varepsilon = \frac{\delta}{L}$ where $F$ is the compressive force, $D$ is the diameter of the micro-pillar tip and $\delta$ and $L$ are the deformation and length of the micro-pillar respectively. The model is calibrated using the 8 strain hardening parameters shown in Table 2.

Material parameters treated as constants are shown in Table 1. The $C_{ij}$ symbols represent the elastic moduli, whereas the Euler angles, which represent the crystal orientation, are specified based on the specific sample being calibrated as no two crystal orientations are alike. Either of the two crystal systems BCC (body-centered cubic) or FCC (face-centered cubic) can be specified in the model. Martensite has a BCT (body-centered tertagonal) structure, but its deviation form the BCC structure is very small. Therefore, this model treats martensite as BCC.

| Parameter | Baseline value |
|---|---|
| `Mat_selector` | Body centered cubic |
| $C_{11}$ | 269,231 |
| $C_{12}$ | 115,385 |
| $C_{44}$ | 76,923.1 |
| $\boldsymbol{\psi = \alpha_1}$ | Depends on experimental data |
| $\boldsymbol{\theta = \alpha_2}$ | Depends on experimental data |
| $\boldsymbol{\varphi = \alpha_3}$ | Depends on experimental data |

*Table 1: Constants defined in the MSU Crystal Plasticity model.*

A filtering procedure, which ensures a monotonic increase of the strain values across all data points, was applied to eliminate two problems encountered in the experimental data:

1. Erratic stress-strain curves which do not have monotonically increasing displacement measurement. This could be problematic for ordinate-based curve matching since there is more than one stress solution for a particular strain value.
2. This remedy also happens to partially address the slip behavior after the yield point. The slip phenomenon is not addressed in the material model, so should ideally be excluded from the data to prevent a false identification.

The filtered curves are shown in Figure 2(b).

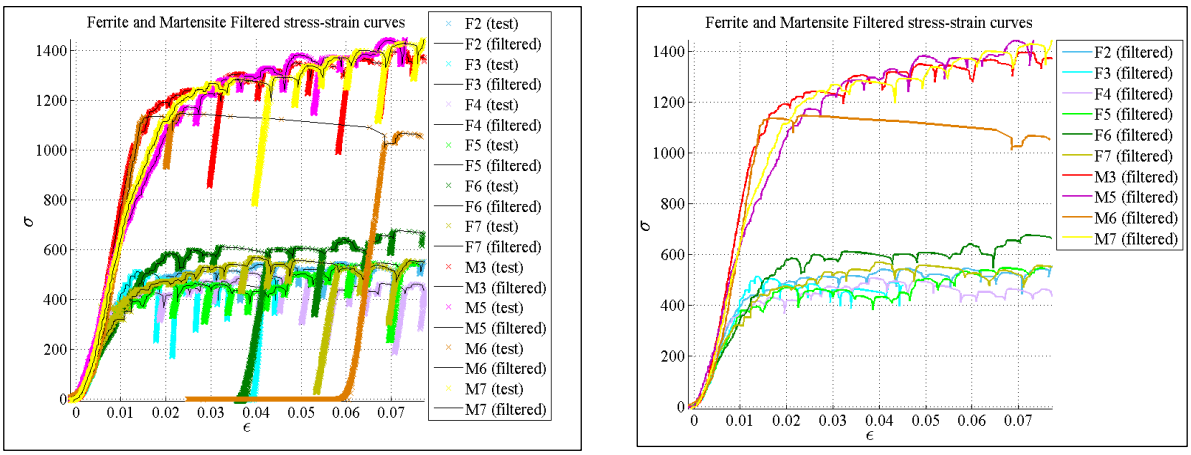


(a) (b)

*Fig.2: (a) Original experimental stress-strain curves of the single crystal Ferrite (F2-F7) and Martensite (M3-M7) phases used in the calibration of the Crystal Plasticity model (provided by Prof. S. Kumar and Dr. H. Ghassemi-Armaki, Brown U.). Each curve represents a different test and hence a different set of Euler angles to orientate the crystal lattice. (b) Results of filtering the original curves. The filtering procedure ensures a monotonic increase of the abscissa values to facilitate the calibration and partially obscures the deep spikes caused by slip behavior not accounted for in the computational model.*

### 4.2 The Finite Element model of the micro-pillar experiment

The Finite Element model of the micro-pillar (MSU) used in the CP model calibration is shown in Figure 3. The model has an elastic base to represent the foundation of the micro-pillar. To model a compression load, a rigid surface is applied at the top.

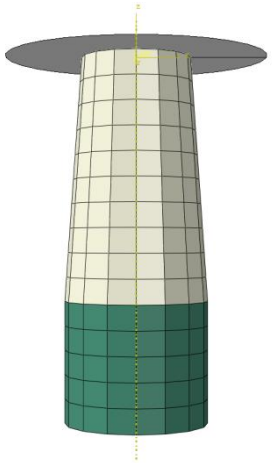

*Fig.3: FE model of the micro-pillar (originally from Prof. Farhang Pourboghrat, MSU) used in the CP calibration. The lower part (dark green) represents an elastic foundation. The base is constrained at the bottom and a downward compressive force is applied at the top.*

An elastic base was introduced by MSU to represent the elastic foundation of the micro-pillar. To address the uncertainty of the elastic properties of the foundation, the Young's Modulus of the elastic foundation was added to the calibration formulation as an optimization variable. The choice of foundation modulus influences the calculation of the deformation (determined by the tip displacement) and therefore also the stress-strain curve.

### 4.3 Calibration results for the CP model

The optimization setup was tested by computing the Mean Squared Error residual based on the ordinate values at the experimental points of each experimental curve and aggregating the results for the phase under consideration. For Martensite, the Euler angles were reported to be the same for all the experiments. Hence only a single simulation was used for each optimization step. For Ferrite, each experiment had a unique set of Euler angles which required a unique input file for each experiment at each optimization step. The BCC-24 crystal plasticity model was used for both phases.

The results for both the martensite and ferrite calibrations are shown in Table 2. Figures 4 and 5 show the comparison of the test and computed results for the calibrated material.

| Parameter | $\tau_{01}$ | $\tau_{02}$ | $\tau_{S1}$ | $\tau_{S2}$ | $h_{01}$ | $h_{03}$ | $a_1$ | $a_2$ |
|---|---|---|---|---|---|---|---|---|
| Ferrite | 170 | 338 | 750 | 613 | 102 | 61.4 | 1.00 | 1.96 |
| Martensite | 485 | 676 | 564 | 942 | 146 | 38.7 | 2.33 | 4.96 |

*Table 2: Final strain hardening parameters for the martensite and ferrite phases using the MSU CP model. These parameters were used as variables in the calibration.*

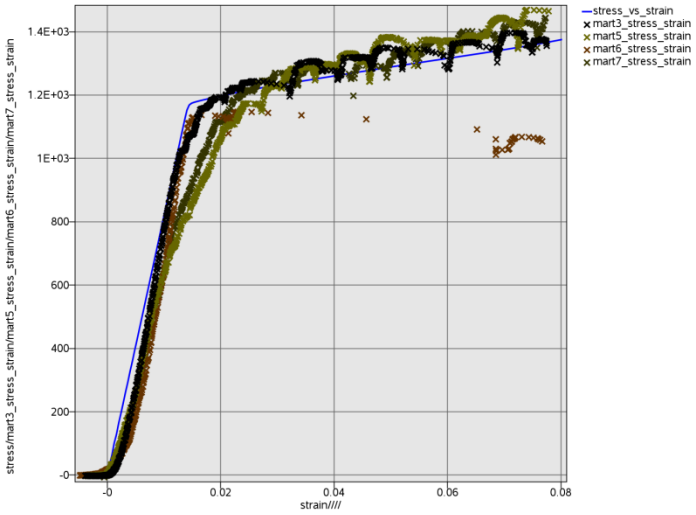


*Fig.4: Final stress-strain histories of the calibrated martensite constitutive model (M3,5,6,7). The crosses represent the experimental results. The blue curve represents the computed stress.*

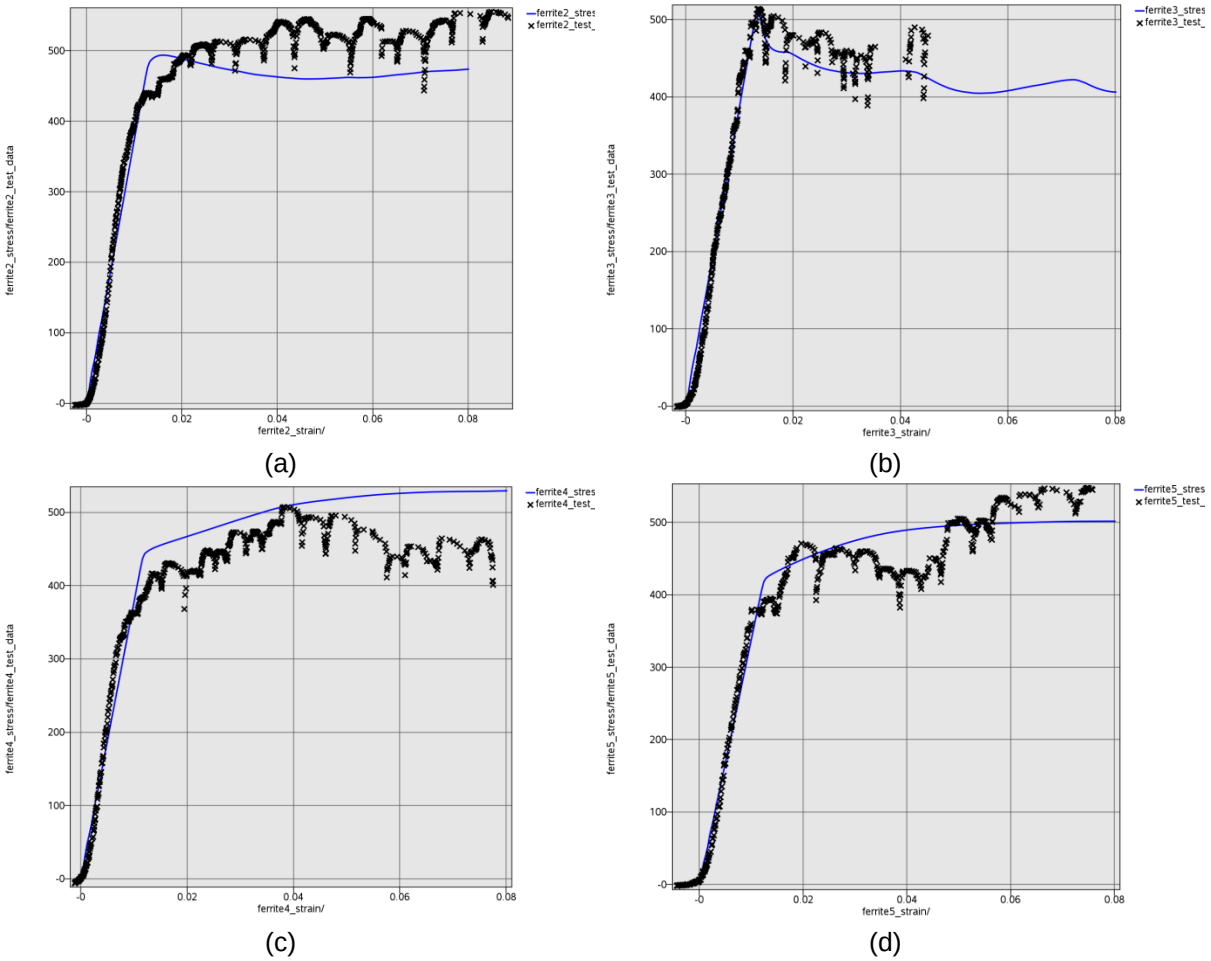


*Fig.5: Final stress-strain histories of the calibrated ferrite constitutive model (F2-5). The crosses represent the experimental results. The blue curve represents the computed stress.*

### 4.4 Remarks

It should be noted that the discrepancies observed in Fig. 4 and Figs. 5 (a)-(d) may partially be because, for each phase, the residual for a unique set of hardening parameters is minimized across all the experiments. A unique set of hardening parameters should therefore be able to represent all the experimental curves for a particular phase. A general mismatch, involving all the curves, can be caused by a single outlier.

It should also be noted that $\tau_{Si} > \tau_{0i}; i = 1,2,3$ as dictated by the CP model theory.

## 5 Calibration of the PNNL State Variable model using LS-DYNA and LS-OPT

The calibration of the State Variable model uses experimental data generated by the in-situ High Energy X-ray Diffraction (HEXRD) test. The experimental data is defined by the retained austenitic volume fraction or the corresponding transformed martensitic volume fraction as a function of equivalent plastic strain. The computed curves are obtained using the Olsen-Cohen model [6].

Five tests are required to calibrate the $a$, $b$ and $n$ constants to produce 5 curves required in the final model. The load states for the five tests are tensile, compression, shear, plane strain and biaxial. The results of the tensile test calibration are shown in Fig. 6 while the corresponding parameter values are shown in Table 3.

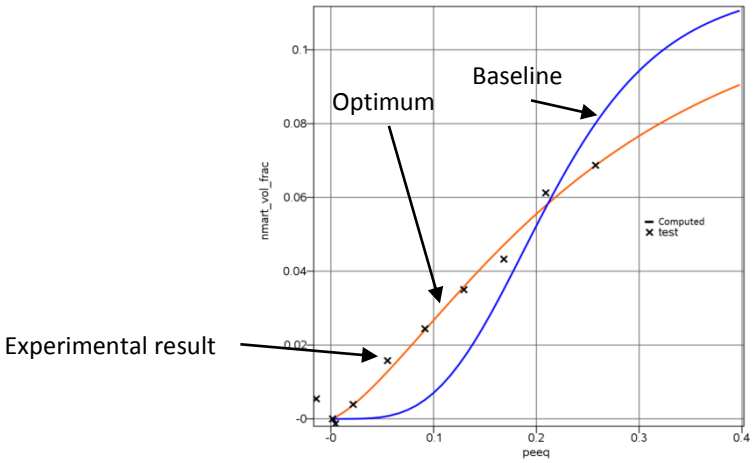


*Fig.6: Results of the calibration of the State Variable model for the tensile test.*

| Experiment type | $a$ | $b$ | $n$ |
|---|---|---|---|
| Tensile | 1.33 | 5 | 1.44 |

*Table 3: Final parameters for the Olsen-Cohen formula for the tensile load case using the State Variable material model. These parameters were used as variables in the calibration.*

## 6 LS-OPT enhancements required for integration

After preliminary tests of the individual calibration components of the overall multi-scale framework, the components were integrated into LS-OPT as shown in Figure 7. Some of the individual components, such as some of the test results for the calibration of the SV model, were not available at the time of writing. However a display of the LS-OPT setup is provided and a detailed description is given in the caption of Figure 7.

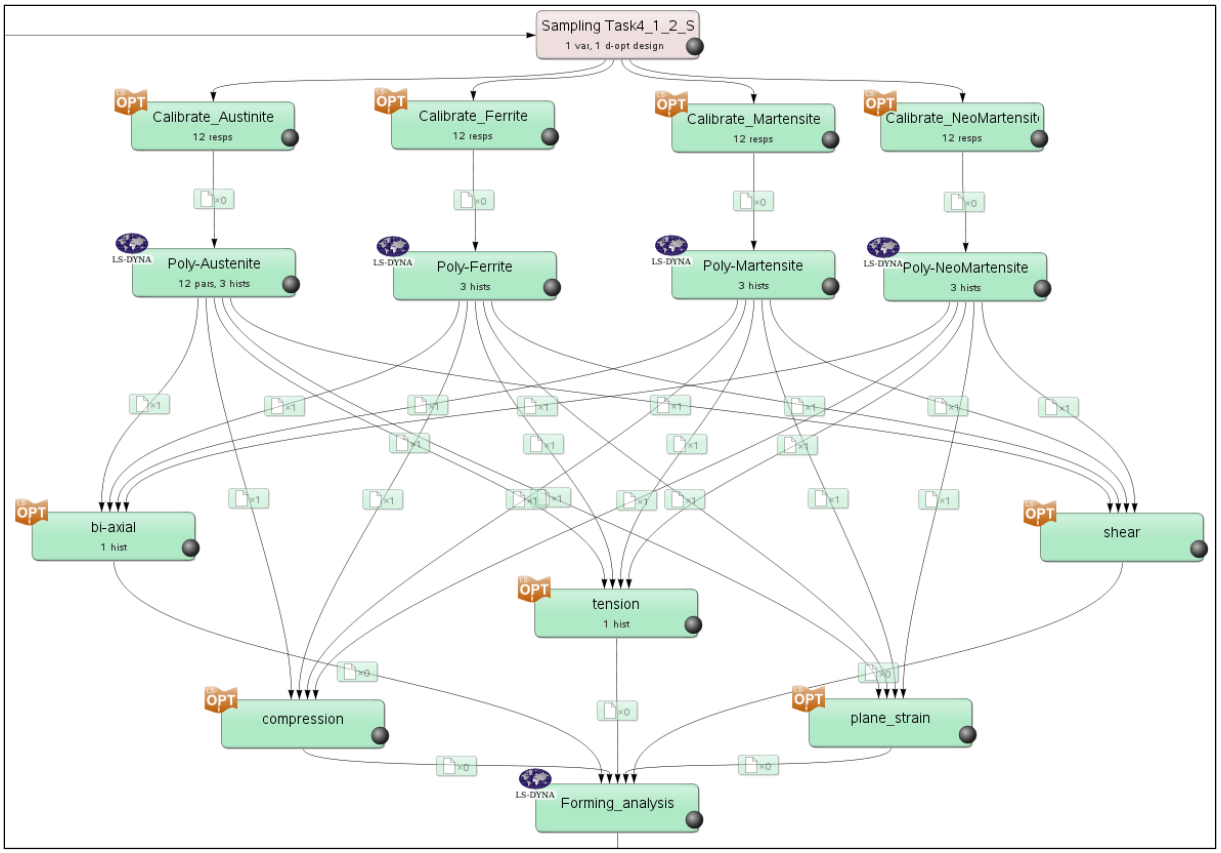


*Fig.7: Multi-level LS-OPT GUI display of the process flow of the integrated multi-scale MSU-CP/PNNL-SV model parameter identification showing (i) identification of the individual CP phases (1st row below Sampling), (ii) polycrystalline analysis of each phase (2nd row) and (iii) PNNL-SV parameter identification for five triaxiality cases. Each box is referred to as a „stage" which is used to define the solver data (solver package, input files) for that stage. Each PNNL-SV parameter identification produces a point on the* $\boldsymbol{a}$, $\boldsymbol{b}$ *and* $\boldsymbol{n}$ *curves to be specified for the forming analysis (last stage). Stages with "OPT" icons represent LS-OPT runs involving sublevel simulations, whereas other stages represent LS-DYNA simulations. The smaller boxes in the flow between (ii) and (iii) represent transfer of stress-strain curves from all the CP to all the SV models (to bridge the length scale gap).*

Several enhancements were added to LS-OPT to facilitate the integration of parameter identification at various levels.

1. A multilevel optimization capability was created by allowing LS-OPT to be defined as a solver or stage type [7] of itself. This allows a multi-level calling structure of infinite depth (at least theoretically). The practical implication is that calibration steps can be scheduled from a master level to integrate the calibration of the State Variable model which requires stress-strain input from individual CP phase calibration steps. Transfer variables were defined so that, in the event that the master level is incorporated into an outer vehicle design optimization loop, variables defined by experimental designs at the outer level can be transferred down as constants to inner levels. Conversely, optimal responses or histories produced at inner levels can be passed to outer levels through extraction.
2. A class of variables named *response variables* [7] was introduced to allow transfer of data between consecutive stages:
    a. The main parameter setup allows the user to link a parameter to a response. This selection causes the selected parameter value to be replaced by a response value produced by a predecessor stage. The transferred response is therefore substituted into the input file of the successor stage.
    b. The response value to be linked can be any value which was directly extracted from a solver database, or it can also be a mathematical expression involving any variables,

dependents, histories or responses defined in any predecessor stages. All functions supported for evaluation at the end of the process flow can be evaluated at any stage in the flow, thereafter to be substituted as a parameter. The evaluation of expressions was thus transferred from the main LS-OPT program to the extractor process.

c. Response variables can be transferred between any two stages of a particular thread. They do not have to be consecutive.
d. A specific response can be linked to any number of downstream parameters.
e. An output history can be flagged to produce a ***DEFINE_CURVE** file which can serve as an include file for LS-DYNA. For example, a stress-strain curve produced by a CP calibration can be passed as a material property to the State Variable calibration.

3. Multilevel navigation features. While setting up or monitoring solver jobs as part of a multilevel optimization, navigating between levels can be a daunting task without automatic navigation features. A system was therefore implemented to automate the following two tasks:
    a. A feature in the Stage dialog to display the input file of an inner level.
    b. A recursive feature in the job progress dialog to select the GUI of an individual lower level process. Once this GUI has been opened, its progress can be selected for viewing.

## 7 Closure

An introductory account of the integration of a multi-scale material calibration using LS-DYNA® and LS-OPT® is given. While the setup process is still in a preliminary stage, it is shown that a micro-scale Crystal Plasticity model can be integrated with a macro-scale State Variable model which can then be used to model metal structures (sheet metal forming, crash simulation). The two material models have been implemented as user materials in LS-DYNA while several features have been added to LS-OPT to facilitate sequencing of the calibration steps and the transfer of variables and responses along the process flow. Some of the individual calibration components have been tested using experimental results from the field.

While the ultimate goal is to conduct an automated multi-scale calibration using LS-OPT, component testing and experimental data acquisition are still under way.

Since the material calibration feature described here represents the material design component of a larger Multidisciplinary Design Optimization (MDO) of a vehicle, several approaches are being contemplated to find a strategy for the integration. Some research ideas are:

1. Construct a model that relates material design variables such as constituent element (e.g. *C*, *Mn*, *Si, Al*, etc.) fractions of the alloys and heat treatment variables to the constitutive parameters. In this way materials can be designed in a continuous space involving the manufacturing process parameters as material design variables. Such a model could be constructed using metamodels.
2. Create a feasible constitutive parameter space by calibrating all the available experiments and using classifiers to bound the parameter space. Material variables are continuous, but can be constrained during optimization by using the classifiers as constraints.
3. Use the tools described in this paper to generate State Variable material models by calibrating a large number of experiments and use Combinatorial Optimization (such as the Genetic Algorithm in LS-OPT [7]) to solve the MDO problem which includes sizing and shape variables. This can possibly be done in a multi-level setting in which the material selection is conducted using a combinatorial algorithm at an inner level. The disadvantage is that a large number of experimental results need to be available before the optimization process can be started, the main advantage being that the optimization yields a solution which has already been physically tested.

## 8 Literature

[1] Integrated Computational Materials Engineering: A Transformational Discipline for Improved Competitiveness and National Security, National Research Council (2008)

[2] Horstemeyer, M., Multiscale Modeling: A Review, *Practical Aspects of Computational Chemistry, ed. J. Leszczynski and M.K. Shukla, Springer Science & Business Media,* pp. 87-135, 2009

[3] Zamiri, A.R. and Pourboghrat, F., A novel yield function for single crystals based on combined constraints optimization, *International Journal of Plasticity, 26, 731-746 (2010)*

[4] Mapar A, Bieler TR, Pourboghrat F, Compton CC. Crystal Plasticity Finite Element Modeling of Single Crystal Niobium Tensile Tests with Weighted Dynamic Hardening Rule, in:. Li M, Campbell C, Thornton K, Holm E, Gumbsch P (Eds.). *2nd World Congr. Integr. Comput. Mater. Eng. TMS (The Minerals, Metals & Materials Society)*; 2013.

[5] Mapar A, Bieler TR, Pourboghrat F, Compton C. Dynamic Hardening Rule; a Generalization of the Classical Hardening Rule for Crystal Plasticity, in:. *16th Int. Conf. RF Supercond. Paris, France*: 2013.

[6] Olsen, G.B. and Cohen, M., Kinetics of strain-induced martensitic nucleation, *Metallurgical Transactions A,* 6(1975) 791-795

[7] Stander, N., Roux, W.J., Basudhar, A., Eggleston, T., Craig, K.-J. *LS-OPT Version 5.1 User's Manual*, June 2014. http://ftp.lstc.com/user/ls-opt/5.1.1/lsopt_51_manual.pdf